Colloids and Surfaces A: Physicochemical and Engineering Aspects 703 (2024) 135201

Contents lists available at ScienceDirect

Colloids and Surfaces A: Physicochemical and Engineering Aspects

journal homepage: www.elsevier.com/locate/colsurfa

Ferrocene-functionalized magnetic core-shell nanoparticles based on hydrosilylation reaction for pH-responsive doxorubicin delivery system

Ali Mohammadzadeh [a], Siamak Javanbakht [a], Reza Mohammadi [a,*], Fahimeh Kazeminava [b]

[a] Polymer Research Laboratory, Department of Organic and Biochemistry, Faculty of Chemistry, University of Tabriz, Tabriz, Iran
[b] Stem Cell Research Center, Tabriz University of Medical Sciences, Tabriz, Iran

HIGHLIGHTS

- Surface modification of Fe_3O_4 with hydrosilylation reaction.
- Fe_3O_4@SiO_2@VTES@Fc/DOX showed a long-time controlled release over 96 h at pH 5.
- Fe_3O_4@SiO_2@VTES@Fc/DOX has a desired pH-responsive DOX delivery property.
- Antioxidant property of the synthesized Fe_3O_4@SiO_2@VTES@Fc nanocarrier.
- Blank Fe_3O_4@SiO_2@VTES@Fc exhibited a cytocompatibility nature toward MCF-7 cells.

GRAPHICAL ABSTRACT

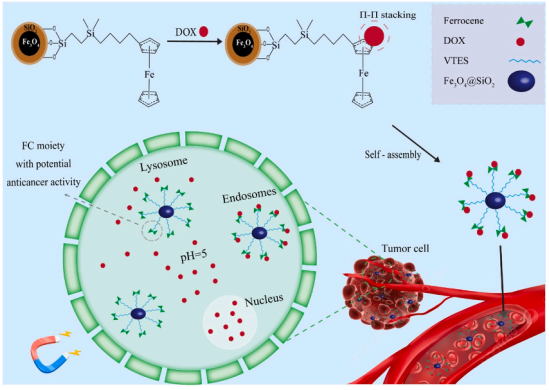

ARTICLE INFO

Keywords:
Magnetic nanoparticle
Hydrosilylation reaction
Ferrocene
Drug delivery system

ABSTRACT

This study describes the development of an innovative pH-sensitive drug delivery system (DDS) utilizing ferrocene (Fc) and magnetic nanoparticles (MNPs) for cancer therapy. One potential method for generating a diverse range of functional NPs involves attaching functional substances to MNPs. In this investigation, we display the successful modification of Fe_3O_4 NPs by an Fc derivative (4-Ferrocenylbutyl)dimethylsilane through a hydrosilylation reaction toward the synthesis of the Fe_3O_4@SiO_2@VTES@Fc nanocarrier (NC). The doxorubicin (DOX) drug was loaded onto Fe_3O_4@SiO_2@VTES@Fc NC with a drug loading capacity of about 80 % via π-π stacking interactions. Also, the prepared materials were thoroughly characterized using FT-IR, XRD, FE-SEM, EDX-MAP, VSM, DAPI, MTT, antioxidants, and CV techniques. In vitro studies on the release of DOX from Fe_3O_4@SiO_2@VTES@Fc NC indicated a pH-responsive behavior with a lower release rate (< 10 %) at pH 7.4 compared to pH 5 (approximately 70 %) over a period of 96 h. Moreover, cytotoxicity assessments demonstrated notable cytotoxic effects of DOX-loaded Fe_3O_4@SiO_2@VTES@Fc on MCF-7 cells (IC50 value: ~8 μg/mL). The study findings suggest that the fabricated magnetic core-shell NC (Fe_3O_4@SiO_2@VTES@Fc/DOX) exhibits stimulus-responsive behavior and holds promise as a sophisticated approach to specifically transport therapeutic agents into tumor sites while minimizing exposure to healthy tissues.

* Corresponding author.
E-mail address: r.mohammadi@tabrizu.ac.ir (R. Mohammadi).

https://doi.org/10.1016/j.colsurfa.2024.135201
Received 12 July 2024; Received in revised form 17 August 2024; Accepted 26 August 2024
Available online 27 August 2024

1. Introduction

The increase in cancer in human societies has caused the use of chemotherapy drugs to increase significantly [1]. The problems of chemotherapy drugs include adverse side effects, the need for high drug doses, and non-specific targeting, which can be solved by designing a targeted drug delivery system (DDS) [2]. Advanced DDS can provide a controlled release of drugs over extended periods, maintaining therapeutic drug levels within the body and avoiding possible side effects that can lead to sub-therapeutic effects or toxicity [3]. Doxorubicin (DOX) is a chemotherapeutic drug often used in the treatment of several cancerous conditions. This drug is placed between the base pairs of the DNA helix, prevents DNA replication, and inhibits protein synthesis [4,5]. Targeted DDS for DOX aims to improve its therapeutic efficacy and reduce toxicity by selectively delivering it to tumor sites [6]. Also, doxorubicin due to having aromatic rings, and hydroxyl and amine groups in its structure, creates π-π interactions, hydrogen and covalent bonds with nanocarriers, respectively. Hence, to enhance treatment outcomes, it is crucial to devise techniques for targeting the medication specifically to the affected area [7].

Nanoscale DDSs have been designed to overcome the drawbacks associated with traditional DDSs, including issues with solubility, bioavailability, and target specificity [8]. These systems can improve the efficacy of drugs by delivering them directly to the target site, reducing side effects [9]. Nanoparticles (NPs) are the primary carriers used in these systems, and they can be made from various materials, including polymers, lipids, and metals [10]. Some of the key advantages of nanoscale drug delivery systems include improved solubility and bioavailability, targeted drug delivery, controlled drug release, passive and active targeting, reduced toxicity, and eco-friendly and biocompatible materials [11]. Meanwhile, magnetic nanoparticles (MNPs) are very favorable in the area of biomedicine owing to their tiny size, prolonged circulation in the body, ability to reduce the negative effects of chemotherapeutic medications, and their function as drug carriers [12].

Iron oxide (Fe_3O_4) MNPs have gained significant interest for their exceptional biocompatibility, non-toxic nature, affordability, ease of surface modification, simple separation, and responsiveness to external magnetic fields. These qualities make them very suitable for many biomedical applications [13]. They have been used in various forms, including core-shell structures to enhance drug delivery efficiency and target specific cells or tissues [14]. The size of Fe_3O_4 MNPs is critical for their use in DDSs [15]. The size of the particles should be more than 10 nm in order to prevent them from being filtered by the kidneys and to ensure slow permeability. However, the size should also be less than 200 nm to avoid being engulfed by the reticuloendothelial system (RES) in the spleen and liver [16,17]. Bare Fe_3O_4 NPs exhibit strong chemical reactivity, rendering them susceptible to oxidation, resulting in the loss of magnetic characteristics in the majority of instances as well as their tendency to aggregate [18]. Surface modification is a prominent technique used to enhance the efficacy of drug NCs which are usually modified with SiO_2, organic and organometallic materials, proteins, and polymers [19]. Meanwhile, Ferrocene (Fc) coating can help increase the stability of nanoparticles and improve their interaction with drug molecules [20].

Fc, a sandwich-like organometallic compound with a planar structure, has been widely used in DDSs due to its unique properties, such as stability, excellent redox properties, and low toxicity [21]. Because Fc has a lipophilic nature, Fc derivatives have an increased ability to penetrate cell membranes [22]. The ferrocenyl group exhibits the remarkable property of undergoing reversible one-electron oxidation through a Fenton-like reaction, resulting in the emission of an electron under physiological conditions [23,24]. This reaction generates the ferrocenium radical cation Fc^{+2} and reactive oxygen species (ROS), which have potential applications in the field of medicinal chemistry [25,26]. These ROS can induce oxidative stress in cancer cells, leading to cell death and enhancing the therapeutic efficacy of the delivered drug [27,28]

In this investigation, we synthesized ferrocenyl-based Fe_3O_4@SiO_2@VTES@Fc core-shell NCs through a hydrosilylation reaction. then DOX as a model anticancer drug was loaded on the Fe_3O_4@SiO_2@VTES@Fc NCs, in which π-π stacking acts as a key role. These interactions entail the non-covalent bonding between aromatic rings, which can be utilized to improve the stability, loading capacity, and release characteristics of DDSs. The incorporation of Fc with Fe_3O_4 nanoparticles can aid in the encapsulation of hydrophobic anticancer medications, like doxorubicin, via π-π stacking interactions.

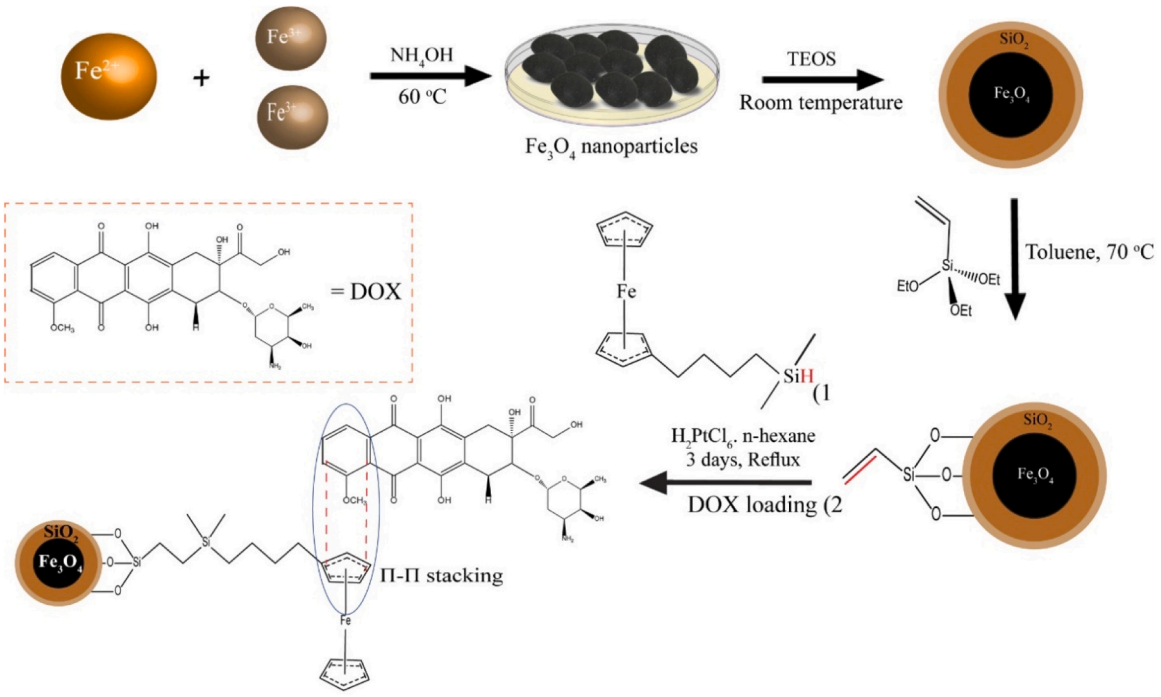

Scheme 1. The representation of the Fe_3O_4@SiO_2@VTES@Fc/DOX preparation.

Additionally, these interactions have the potential to bolster the stability of the drug-carrier combination, thereby averting premature drug release. Ultimately, the drug's release behavior, drug release kinetics, and the MTT test were examined under controlled conditions in the laboratory environment. Scheme 1.

2. Experimental

2.1. Materials

$FeCl_2.4\ H_2O$, $FeCl_3.6\ H_2O$, NH_4OH (25 %), Vinyltriethoxysilane (VTES, 99 %), tetraethyl orthosilicate (TEOS, 99 %), *n*-hexane (99 %), *N*-methyl-2-pyrrolidone (NMP, 98 %), ethanol (99 %), H_2SO_4 (98 %), H_2PtCl_6 (99 %), 2,2 diphenyl-1-picrylhydrazyl (DPPH), and 3-(4,5-dimethyl thiazole-2-yl)-2,5-diphenyl tetrazolium bromide (MTT) were purchased by Sigma-Aldrich Co. and utilized without additional purification, as well as the doxorubicin hydrochloride (DOX) was obtained from Sobhan Pharmaceuticals Co. (Iran).

2.2. Characterization

Fourier transform Infrared (FT-IR) spectra were recorded using an FT-IR spectrometer (Bruker Instruments, model Aquinox 55, Germany) with a scanning range of 4000–400. X-ray diffraction (XRD) measurements were performed using a Siemens D500 instrument with Cu-Ka radiation at 35 Kv. The FE-SEM and EDX analyses were conducted using a TESCAN MIRA3 instrument at an acceleration voltage of 15 kV. The magnetic properties of the prepared materials were evaluated using a vibrating sample magnetometer (VSM) from LDJ (model 9600–1, USA). The Shimadzu 1700 spectrophotometer was used to conduct ultraviolet-visible (UV-Vis) absorption spectra.

2.3. Synthesis of Fe_3O_4@SiO_2@VTES@Fc

Fe_3O_4@SiO_2@VTES@Fc was synthesized according to our reported method [29]. Briefly, For the synthesis of Fe_3O_4 MNPs, 3.96 g (20 mmol) $FeCl_2{\cdot}4\ H_2O$, 10.82 g (40 mmol) $FeCl_3{\cdot}6\ H_2O$, and 320 mL of ionized water were added in a round bottom flask and mixed under nitrogen gas and mechanical stirrer. Subsequently, 40 mL of NH_4OH was slowly added to the resulting mixture. After the pH of the reaction environment reached 11, the reaction mixture was stirred at 60°C for 8 h. Finally, the synthesized Fe_3O_4 MNPs were collected using an external magnetic field and washed 4 times with deionized water and ethanol.

in continuing, 1 g of synthesized Fe_3O_4 MNPs was dispersed in a mixture of 40 mL of ethanol, 160 mL of deionized water, and 4 mL of aqueous ammonia solution. Additionally, 4 mL of TEOS was added to the mixture, which was then stirred for 4 h at room temperature. The silica-coated Fe_3O_4 MNPs (Fe_3O_4@SiO_2) were subsequently isolated using an external magnet and were thoroughly washed with ethanol.

In the next step, for the synthesis of Fe_3O_4@SiO_2@VTES, first, 1 g of Fe_3O_4@SiO_2 was dispersed in 50 mL of dry toluene, and then 2 mL of VTES was added drop by drop to the resulting suspension and stirred for 24 h at 70 °C. Finally, Fe_3O_4@SiO_2@VTES MNPs were collected using an external magnetic field and washed several times with ethanol.

To facilitate the incorporation of the Fc derivative onto the surface of Fe_3O_4@SiO_2@VTES, a grafting reaction was conducted in dry *n*-hexane as the solvent, utilizing a hydrosilylation reaction in the presence of Karstedt's catalyst. Precisely, 0.500 g of Fe_3O_4@SiO_2@VTES NPs were evenly dispersed in dry *n*-hexane using an ultrasonic bath. Subsequently, 0.500 g of (4-Ferrocenylbutyl)dimethylsilane synthesized according to our previous work [30], was added to the resultant suspension. Then, the reaction mixture was refluxed for 72 h after the addition of Karstedt's catalyst. Ultimately, following the collection of the ferrocenyl-modified magnetic nanoparticles and their subsequent washing with *n*-hexane, the final product was obtained.

2.4. DOX loading in the Fe_3O_4@SiO_2@VTES@Fc

First, 100 mg of Fe_3O_4@SiO_2@VTES@Fc and 10 mg of DOX (2 mg/mL) were dispersed in phosphate-buffered saline (PBS, pH 7.4) for 20 min. Subsequently, the samples were agitated for 48 h in a light-free environment at room temperature. After the specified duration, the DOX-loaded Fe_3O_4@SiO_2@VTES@Fc were collected using an external magnet and then washed with PBS (pH 7.4) to eliminate the drugs that had been adsorbed onto the surface of the Fe_3O_4@SiO_2@VTES@Fc. Ultimately, it was dried at room temperature. Furthermore, from the supernatant solution of the collected nanoparticles, the amount of loaded DOX was calculated using UV-Vis spectroscopy at 480 nm to determine the drug loading efficiency (DLE) and drug encapsulation efficiency (DEE). In order to get the DEE and DLE values, we employed the following equations: (1) and (2) [31,32].

$$DEE(\%) = \frac{(Amount\ of\ drugs\ in\ nanocarriers(mg))}{(Initial\ amount\ of\ drugs(mg))} \times 100 \quad (1)$$

$$DLE(\%) = \frac{(Amount\ of\ drugs\ in\ nanocarriers(mg))}{(Amount\ of\ nanocarriers(mg))} \times 100 \quad (2)$$

2.5. In vitro DOX release experiment

For the purpose of studying DOX release behavior, a solution containing 10 mg of DOX-loaded NCs (Fe_3O_4@SiO_2@VTES@Fc/DOX) was dispersed with 10 mL of PBS and sodium acetate buffer (SAB), with pH values of 7.4 and 5, respectively. At various intervals, they were placed in a shaking incubator at 37 °C. After that, at the specified intervals, 2 mL of the drug-containing aqueous solution was removed and replaced with an equal volume of fresh buffer to maintain a consistent volume. The amount of DOX released by the Fe_3O_4@SiO_2@VTES@Fc/DOX was ascertained using a preset calibration curve and UV-Vis spectroscopy at a wavelength of 480 nm. The percentages of released DOX were determined by using Eq. (3) [33,34].

$$Released\ drug(\%) = \frac{(Cumulative\ weight\ of\ released\ DOX(mg))}{(Total\ weight\ of\ loaded\ DOX(mg))} \times 100 \quad (3)$$

2.6. Antioxidant assay

The DPPH free radical scavenging activity of Fe_3O_4@SiO_2@VTES@Fc NCs was evaluated according to the procedure outlined by Arlorio, Coïsson, Travaglia, Gindro, Rinaldi, and Locatelli (2009), with slight modifications. Briefly, various concentrations (1–15 μg/mL) of Fe_3O_4@SiO_2@VTES@Fc NCs were exposed to 1 mL of DPPH radical solution (25 mg dissolved in 1000 mL of ethanol), vigorously shaken in the dark at room temperature for 60 min. The UV-Vis absorbance of the samples was recorded at 517 nm against an ethanol blank. The antioxidant effectiveness of the samples was quantified as a percentage of DPPH radical inhibition using the following formula Eq. (4) [35].

$$Inhibition(\%) = \frac{(A_{control} - A_{sample})}{A_{control}} \times 100 \quad (4)$$

$A_{control}$ is the value of the DPPH absorbance, and A_{sample} is the absorbance value of the test solution.

2.7. Cytotoxicity study

The cytotoxicity of the DOX-loaded Fe_3O_4@SiO_2@VTES@Fc NCs was evaluated using the MTT assay on breast cancer MCF-7 cell lines. In summary, MCF-7 cell lines were selected and seeded in 96-well plates at a density of 8000 cells per well in 200 μL of cell culture medium. The plates were then incubated overnight at 37 °C. Then, the MCF-7 cells were exposed to varying concentrations of free DOX,

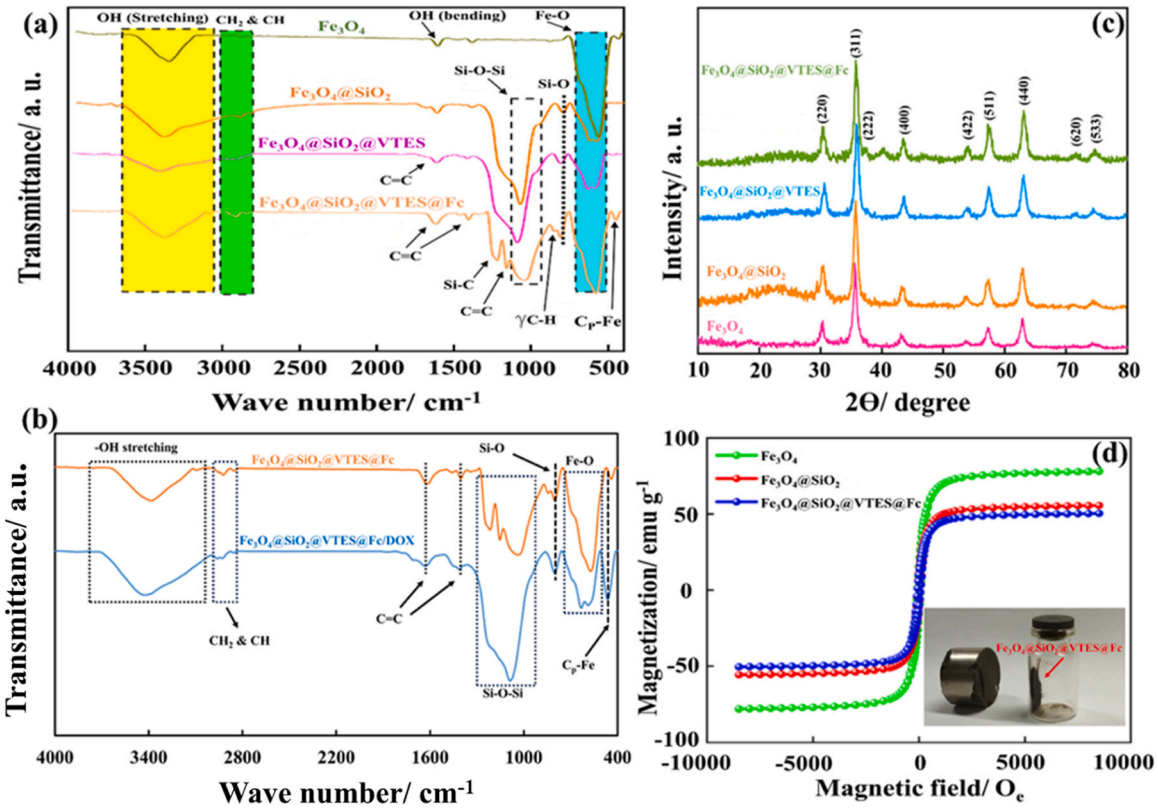

Fig. 1. Fig. 1 (a), (b) FT-IR spectra (c) The XRD patterns, and (d) The VSM curves of as-prepared nanoparticles (reproduced from reference [29]. Reprinted with permission from Elsevier)

Fe_3O_4@SiO_2@VTES/DOX, and Fe_3O_4@SiO_2@VTES@Fc/DOX with respect to the DOX concentration, followed by a 48 h incubation period in a light-deprived setting. In addition, to assess their biocompatibility, cells were exposed to blank Fe_3O_4@SiO_2@VTES@Fc NCs. The cell cytotoxicity was investigated by replacing the culture medium with 20 μL of MTT solution at a concentration of 5 mg/mL, added to the 150 μL of fresh culture medium in each well. 200 μL of dimethyl sulfoxide (DMSO) was introduced to the growing medium 4 h later at 37 °C in order to dissolve the formazan crystals. For every experiment, three separate runs were conducted [36].

2.8. DAPI staining

To evaluate the efficacy of the nanocarrier for biomedical fields, cellular absorption of Fe_3O_4@SiO_2@VTES@Fc/DOX and free DOX was examined using a fluorescent microscope. Human cells were seeded in 24-well plates, treated with Fe_3O_4@SiO_2@VTES@Fc/DOX and free DOX at IC50 concentration determined from the MTT assay, and then incubated at 37 °C for 24 h. After washing with PBS, cells were fixed with 4 % paraformaldehyde at 25 °C for 15 min, stained with DAPI in the dark, and imaged with a fluorescence microscope [37].

3. Results and discussion

3.1. FT-IR, XRD, and VSM analyses

The FT-IR technique was utilized to assess the surface functional groups of the synthesized materials, with the resulting spectra depicted in Fig. 1. The FT-IR spectrum of Fe_3O_4 NPs exhibited absorption bands at 574 cm^{-1}, 1625 cm^{-1}, and 3387 cm^{-1}, corresponding to the stretching vibration of Fe-O bands, the bending vibration of O-H groups, and stretching vibration of O-H bands, respectively. In the spectrum of Fe_3O_4@SiO_2, a prominent absorption band at 1084 cm^{-1} indicated the asymmetric stretching vibration of Si-O-Si, while a peak at 791 cm^{-1} was characteristic of Si-O, confirming successful surface modification with SiO_2 [38,39]. The appearance of peaks at 1642 cm^{-1} in the FT-IR spectrum of Fe_3O_4@SiO_2@VTES suggested the presence of C═C vibrations, confirming effective grafting of the silane coupling agent [40]. Furthermore, the FT-IR spectrum of Fe_3O_4@SiO_2@VTES@Fc revealed new peaks at 465 cm^{-1}, 802 cm^{-1}, 1154 cm^{-1}, 1415 cm^{-1}, and 1643 cm^{-1}, associated with Cp-Fe, γC-H, and C═C bands, indicating successful modification of the MNPs surface with the Fc moiety. According to Fig. 1b, after loading the DOX drug on the Fe_3O_4@SiO_2@VTES@Fc NCs, the stretching vibration intensity of the -OH bands and C_p-Fe has increased, which indicates the effect of these groups in successful loading of the DOX drug on the NCs. On the other hand, π-π stacking and H-bonding are the most possible interactions in DOX loading onto Fc [41]. These results provided strong evidence for the stepwise modification of MNP and DOX loading on NCs.

The produced nanomaterials' crystalline structure was assessed using the room-temperature XRD method with Cu-Kα1 radiation. Fig. 1c displays the XRD patterns of the Fe_3O_4, Fe_3O_4@SiO_2, Fe_3O_4@SiO_2@VTES, and Fe_3O_4@SiO_2@VTES@Fc NCs. The diffraction peaks observed at specific angles (2θ) such as 18.1, 30.8, 35.6, 37.0, 43.2, 53.9, 57.4, 62.8, 71.9, and 74.8 correspond to the (111), (220), (311), (222), (400), (422), (511), (440), (620), and (553) reflections of Fe_3O_4 [42]. The existence of distinct peaks indicates the effective formation of pure Fe_3O_4 with an inverse-spinal structure, whereas the lack of peaks due to contaminants confirms their absence. The XRD patterns of Fe_3O_4@SiO_2 and Fe_3O_4@SiO_2@VTES samples also displayed these distinctive peaks, with the exception of a broadened peak in the 2θ range of 20°-30° attributed to the amorphous SiO_2 layer. This indicates that the phase structure of MNPs remained intact after the formation of the SiO_2 outer layer. Additionally, the XRD pattern of Fe_3O_4@SiO_2@VTES@Fc, as shown in Fig. 1c, displayed similar diffraction peaks, suggesting the robustness of magnetite NPs throughout the

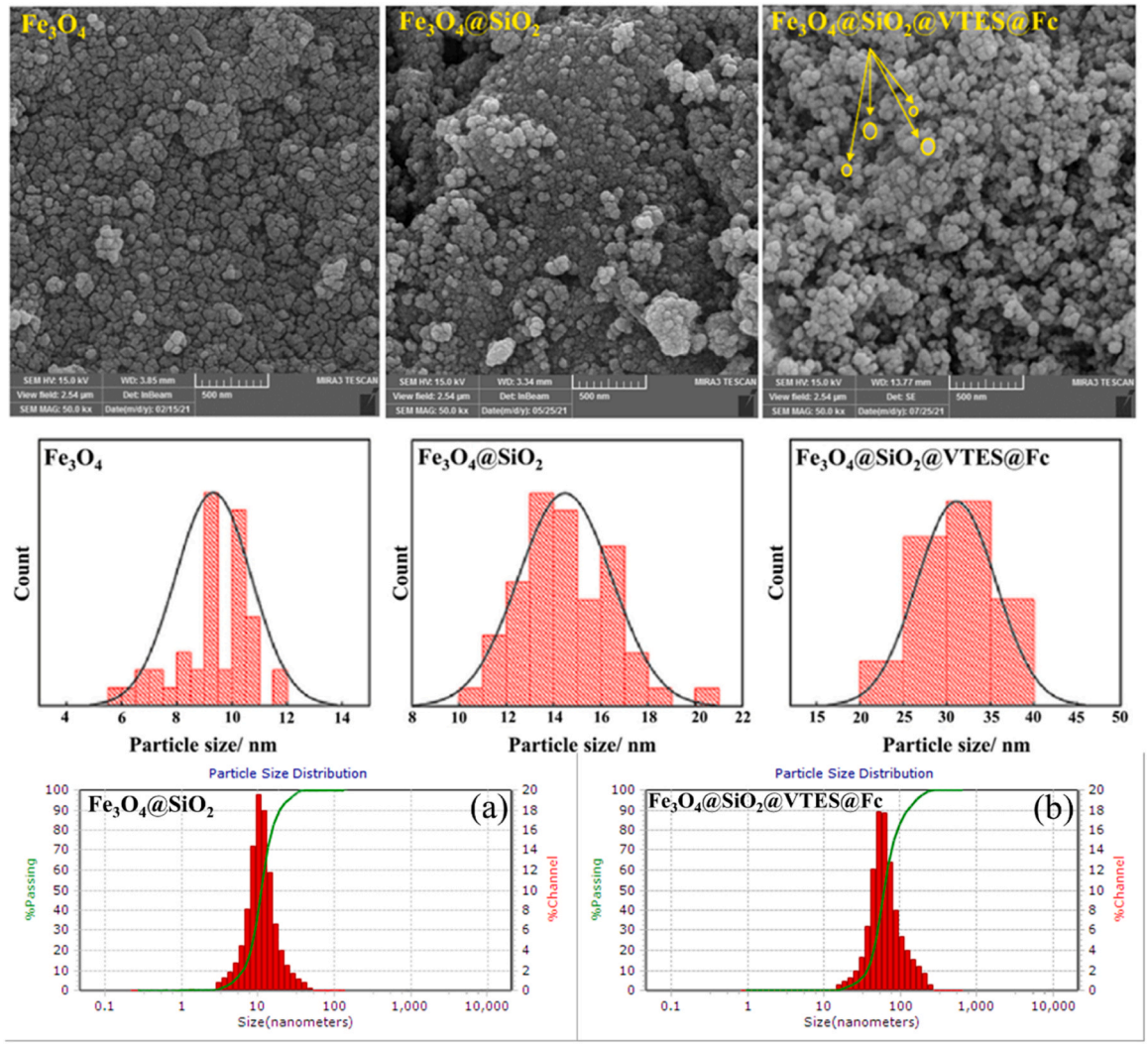

Fig. 2. Fig. 2 FE-SEM images, particle size distribution histograms, and (a), (b) DLS analysis (reproduced from reference [29]. Reprinted with permission from Elsevier).

coating procedure. The Fc diffraction peaks were generally undetectable, except for a small peak near 40°, indicating a possible overlap with the intense diffraction of the amorphous silica.

The VSM profiles of the synthesized NPs are depicted in Fig. 1d. As illustrated in Fig. 1d, the graphs demonstrate a reduction in the saturation magnetization values to 79 emu g^{-1}, 55 emu g^{-1}, and 51 emu g^{-1} for Fe_3O_4, Fe_3O_4@SiO_2, and Fe_3O_4@SiO_2@VTES@Fc, respectively. The decline of the magnetic power of Fe_3O_4@SiO_2@VTES@Fc is attributed to the nonmagnetic SiO_2 and Fc compounds coated on the Fe_3O_4 surface. Upon concentrating magnetic nanoparticles (MNPs) at the desired therapeutic site, the implementation of an alternating magnetic field can induce localized heating of these MNPs through a process known as magnetic hyperthermia. This localized increase in temperature can trigger the release of drug from temperature-sensitive carriers, facilitating a controlled release mechanism specific to the target area. Furthermore, the generated heat can disrupt the structural integrity of nanocarriers, thereby enhancing the release of the encapsulated drugs precisely at the intended location. One of the predominant mechanisms underlying magnetically triggered drug release is the magnetic oscillation of MNPs induced by a pulsating magnetic field. This oscillation generates mechanical forces that can compromise the lipid bilayer of cellular membranes, leading to the subsequent release of drugs within cancer cells targeted by the delivered MNPs. The interaction between the oscillating magnetic field and the magnetic nanoparticles can facilitate permeability alterations or even membrane disruption, thereby enabling efficient drug delivery directly at the cellular level. [43]. Magnetic carriers can provide a protective environment for drugs, protecting them from degradation before they reach their target site. This is particularly important for sensitive biologics or chemotherapeutic agents that may degrade in the bloodstream. Also, these carriers can improve the uptake of drugs into target cells. The application of an external magnetic field can increase the local concentration of the drug near the cellular membrane, potentially enhancing the internalization of the drug by cells through mechanisms such as endocytosis [44,45].

3.2. SEM, EDX, and DLS analyses

The surface morphology of the NPs that were synthesized was examined using the FE-SEM method. Before conducting the FE-SEM investigation, a thin coating of gold (Au) was placed on the materials using the sputtering technique to minimize sample charging. According to Fig. 2, All of the NP samples that were generated demonstrate a consistent and symmetrical spherical shape. The NPs that were synthesized were analyzed for size using Image J software, and the resulting histograms are shown in Fig. 2. Furthermore, the growth in particle size following each modification step was validated through these histograms. This contribution can confirm the successful functionalization of

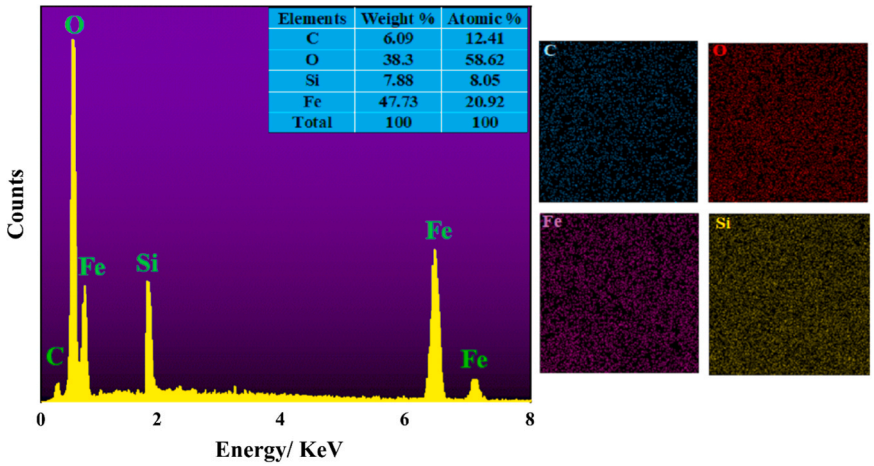

Fig. 3. Fig. 3 (a) The EDX results of the Fe3O4@SiO2@VTES@Fc NCs (reproduced from reference [29]. (b) Reprinted with permission from Elsevier).

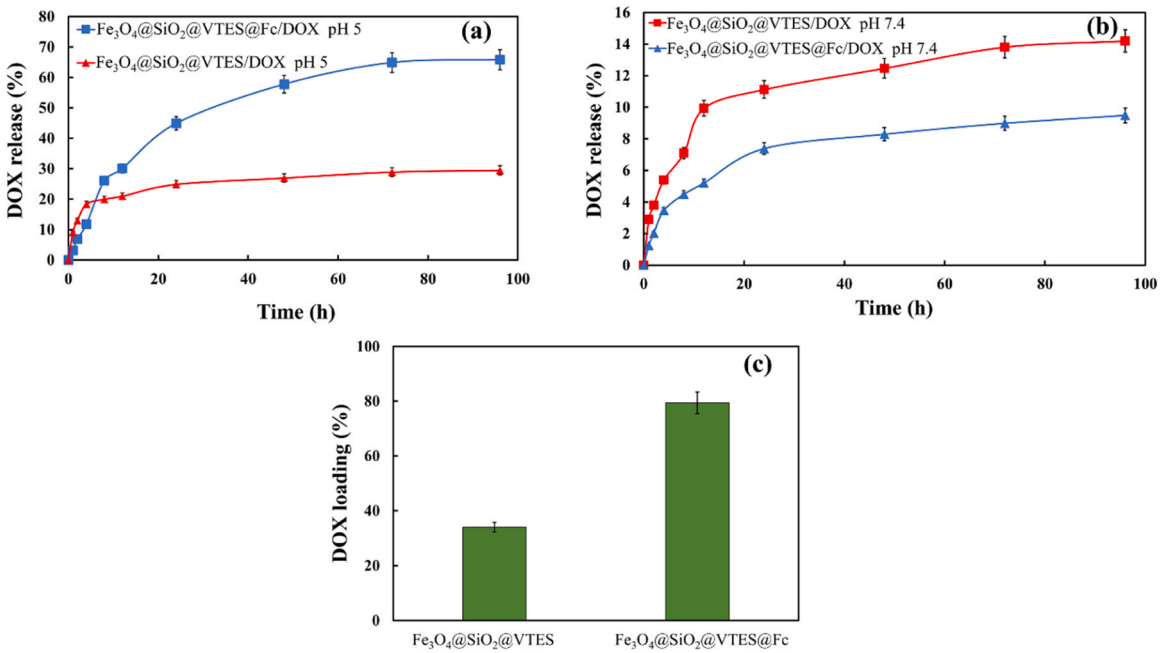

Fig. 4. DOX loading (c) and its cumulative release from Fe_3O_4@SiO_2@VTES@Fc/DOX and Fe_3O_4@SiO_2@VTES/DOX at pH 7.4 in 37 °C.

Fe_3O_4 NPs. The estimated average diameters of the Fe_3O_4, Fe_3O_4@SiO_2, and Fe_3O_4@SiO_2@Fc NPs were approximately 10 nm, 15 nm, and 30 nm, respectively [46]. Fig. 2a, b illustrates the average sizes of Fe_3O_4@SiO_2 and Fe_3O_4@SiO_2@VTES@Fc NCs, as determined by DLS analysis, which is about 12 nm and 75 nm, respectively. Particles within the range of 100–200 nm are well-suited for use as drug carriers, as they minimize rapid renal clearance and uptake by the reticuloendothelial system while facilitating the targeting of specific tissues, such as tumors, via external magnetic fields [47].

EDX analysis is a valuable method for qualitatively assessing the elemental composition and distribution within a sample. The EDX spectrum of the ferrocenyl-modified MNPs demonstrates the presence of C (6.09 %), O (38.3 %), Si (7.88 %), and Fe (47.73 %) elements (Fig. 3). The identification of these elements confirms the successful modification of the MNPs.

3.3. Electrochemical characteristics of the Fe_3O_4@SiO_2@VTES@Fc

Electrochemical measurements were performed to evaluate the electrochemical characteristics of the prepared Fe_3O_4@SiO_2@VTES and Fe_3O_4@SiO_2@VTES@Fc NCs. CV measurements were conducted at a scan rate of 10 mV s^{-1}, and their resulting curves are illustrated in Fig. 5a. Fe_3O_4 MNPs coated with ferrocenyl (Fe_3O_4@SiO_2@VTES@Fc) demonstrate exceptional electrochemical performance in their CV response. The greater enclosed area of the CV curve of Fe_3O_4@SiO_2@VTES@Fc NCs suggests that their redox characteristics are better than those of Fe_3O_4@SiO_2@VTES NPs, as seen in the CV data, which indicates the successful surface modification of Fe_3O_4 MNPs by ferrocenyl.

3.4. In vitro DOX loading and release studies

To assess the efficacy of the synthesized nanocarrier as a drug carrier, DOX was used as a model drug to examine its loading capacity and release profiles. At a weight ratio of 1:10 between DOX and the NCs, the DEE of DOX was determined to be 79.3 ± 0.5 % for Fe_3O_4@SiO_2@VTES@Fc and 34.7 ± 0.5 % for Fe_3O_4@SiO_2@VTES (Fig. 4c). The higher loading of DOX in the Fe_3O_4@SiO_2@VTES@Fc NCs is

Table 1
Results of DOX release kinetics.

Kinetic models	Equation	Coefficient of determination (R^2)			
		Fe_3O_4@SiO_2@VTES@Fc		Fe_3O_4@SiO_2@VTES	
		pH 7.4	pH 5	pH 7.4	pH 5
Zero-order	$F= k_0.t$	0.642	0.91	0.521	0.486
First-order	$\ln(1-F) = k_f.t$	0.640	0.908	0.517	0.685
Higuchi	$F= k_H.t^{1/2}$	0.816	0.839	0.696	0.739
Weibull	$\ln[-\ln(1-F)] = -ß \ln t_d + ß \ln t$	0.971	0.978	0.987	0.922

NOTE: F is the portion of drug release. Ln is the natural logarithm. k_f, and k_H are the kinetic constants of related models.

attributed to the surface modification of the Fe_3O_4@SiO_2@VTES NPs by Fc and also to the possible π-π stacking interactions between DOX and Fc [48]. About 65 ± 0.5 % of DOX drugs from Fe_3O_4@SiO_2@VTES@Fc and about 30 ± 0.5 % from Fe_3O_4@SiO_2@VTES NCs were released at pH 5 for 96 h. As shown in Fig. 4a, the drug release for the Fe_3O_4@SiO_2@VTES@Fc occurs at a controlled and sustained rate, which could be as a result of its π-π stacking interactions. In contrast, for the Fe_3O_4@SiO_2@VTES/DOX, the drug release rate is explosive due to the absence of these interactions. Significantly, this characteristic results in the lowest release rate for Fe_3O_4@SiO_2@VTES@Fc/DOX at pH 7.4 (Fig. 4b), providing an advantage by minimizing potential side effects of DOX on the body's physiological systems.

Additionally, the in vitro release of DOX was analyzed using four different kinetic models for the Fe_3O_4@SiO_2@VTES and Fe_3O_4@SiO_2@VTES@Fc NCs. The Weibull model was found to be the most reliable model for the release of DOX from Fe_3O_4@SiO_2@VTES and Fe_3O_4@SiO_2@VTES@Fc in pH 7.4 and pH 5. This indicated that the release profile of the drug is followed by the diffusion mechanism, as shown in Table 1. All the results indicated that the developed Fe_3O_4@SiO_2@VTES@Fc/DOX NCs offered a promising outcome for sustained release of the anticancer DOX drug in the acidic environment of tumor cells.

3.5. Antioxidant properties of the Fe_3O_4@SiO_2@VTES@Fc

The DPPH method was used to investigate the antioxidant activity of the Fe_3O_4@SiO_2@VTES@Fc NCs. The results are shown in Fig. 5b, c, and d. As illustrated in Fig. 5d, the DPPH peak intensity at 517 nm diminishes as the concentration of the Fe_3O_4@SiO_2@VTES@Fc NCs increases [49]. There was a correlation between the heightened antioxidant performance and the decreased absorption of the samples, indicating a dose-dependent relationship with the Fe_3O_4@SiO_2@VTES@Fc NCs. Fig. 5b shows the % radical scavenging activity of the Fe_3O_4@SiO_2@VTES@Fc NCs. The findings indicate that the Fe_3O_4@SiO_2@VTES@Fc displays remarkable antioxidant properties. The enhanced antioxidant activity observed for the Fe_3O_4@SiO_2@VTES@Fc NCs can be attributed to the redox property of Fc. This redox behavior allows Fc to participate effectively in electron transfer processes, which is crucial for scavenging free radicals.

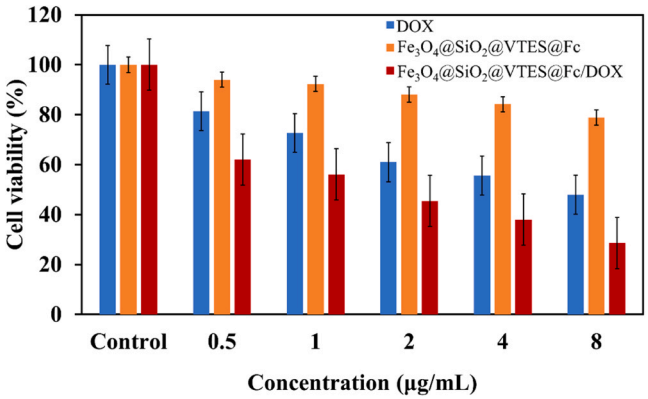

Fig. 6. MTT assay of Fe_3O_4@SiO_2@VTES@Fc/DOX, Fe_3O_4@SiO_2@VTES@Fc, and free DOX on MCF-7 cells in various concentrations.

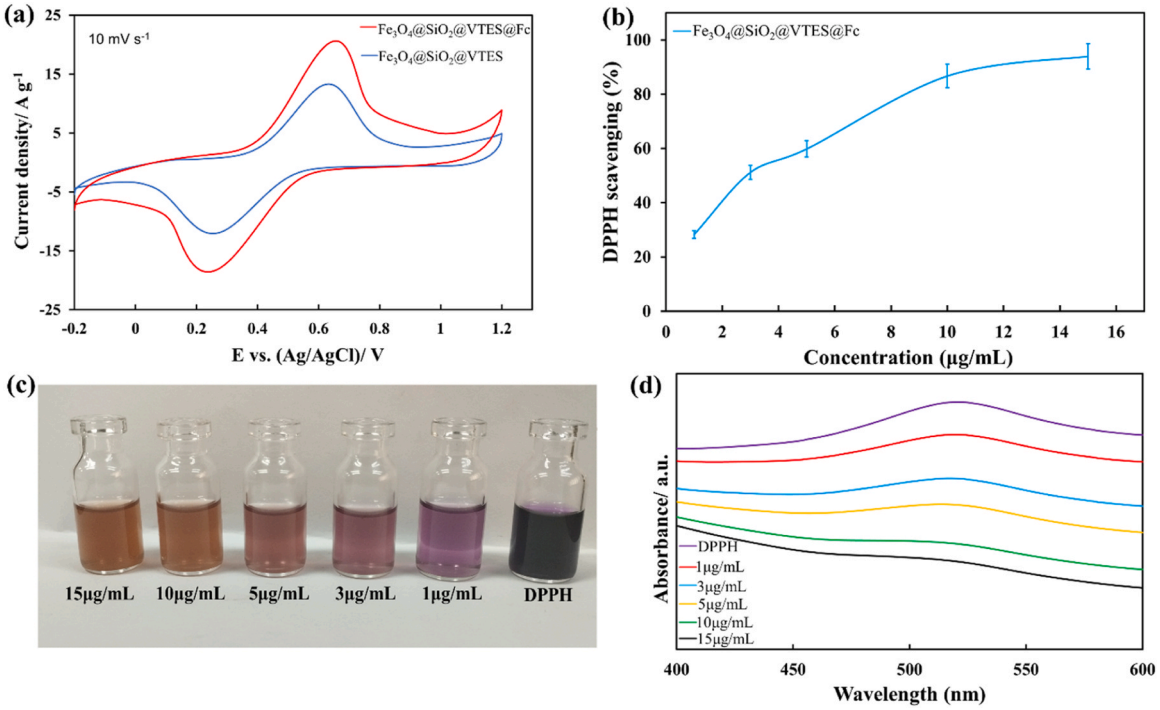

Fig. 5. (a) The CV curves of the Fe_3O_4@SiO_2@VTES@Fc nanoparticle at 10 mV s^{-1} scan rate, (b) DPPH scavenging by Fe_3O_4@SiO_2@VTES@Fc, (c) Photograph illustrating the antioxidant activity, and (d) UV-Vis spectra of Fe_3O_4@SiO_2@VTES@Fc in 1–15 µg/mL concentrations to assess antioxidant activity with DPPH assay.

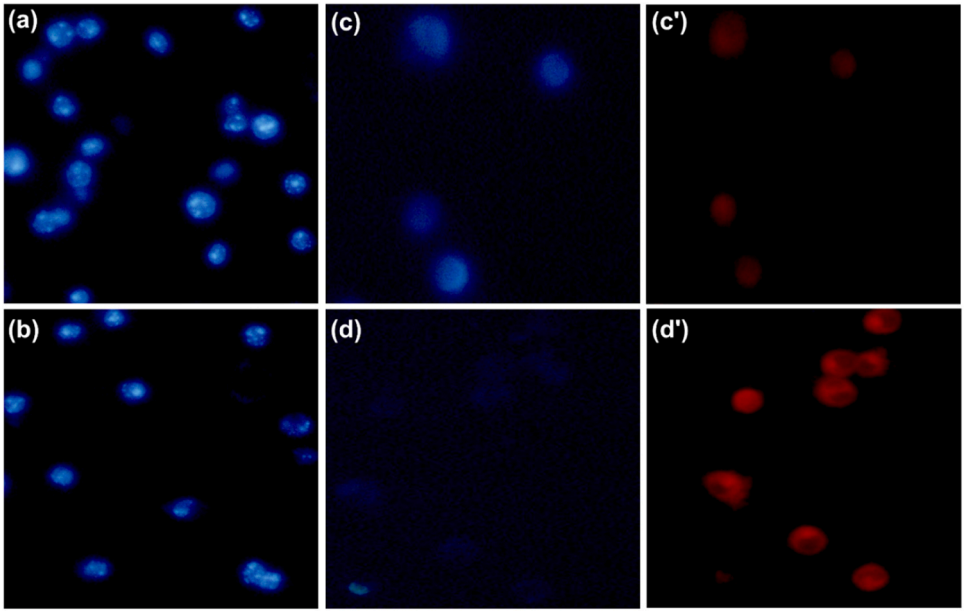

Fig. 7. DAPI staining of incubated MCF-7 cells with untreated cells as control (a); After treatment with Fe_3O_4@SiO_2@VTES@Fc (b), Fe_3O_4@SiO_2@VTES@Fc/DOX (c) (c′:DOX-related image) and Free DOX (d) (d′: DOX-related image) for 48 h.

3.6. MTT assay

The cytotoxicity and cytocompatibility of the synthesized NCs were evaluated using the MTT assay on MCF-7 cells. Based on Fig. 6, the Fe_3O_4@SiO_2@VTES@Fc NCs exhibited minimal cytotoxic effects on MCF-7 cells, with cell viability of > 90 % at a concentration of 1 μg/mL. This observation provides evidence of favorable cytocompatibility and resistance to anticancer drug delivery systems. In contrast, MCF-7 cells showed cytotoxic effects when exposed to DOX-loaded Fe_3O_4@-SiO_2@VTES@Fc NC. The cytotoxicity of DOX-loaded Fe_3O_4@-SiO_2@VTES@Fc NCs was higher compared to free DOX in its equal concentration. The increased cytotoxicity noted in DOX-loaded Fe_3O_4@SiO_2@VTES@Fc can likely be ascribed to the nanoscale dimensions of the synthesized NCs, which enabled facile penetration into cancerous tissues and subsequently amplified the drug's cytotoxic effects [50]. The findings demonstrated that the synthesized Fe_3O_4@-SiO_2@VTES@Fc/DOX exhibits significant potential as an effective NC for anticancer DDSs.

3.7. DAPI staining

To further assess the outcomes of the MTT analysis, a fluorescence imaging study was carried out on MCF-7 cells exposed to different treatments. DAPI is a reliable technique for analyzing cell apoptosis as it specifically attaches to cell nuclei, enabling visualization through fluorescence imaging. In this study, changes in the nuclear structure of the MCF-7 cell line were analyzed by DAPI staining in conjunction with fluorescence microscopy. The MCF-7 cancer cells were treated with Fe_3O_4@SiO_2@VTES@Fc, Fe_3O_4@SiO_2@VTES@Fc/DOX, free DOX, and untreated control cells. The images acquired following DAPI staining displayed a greater proportion of cells when utilizing the Fe_3O_4@-SiO_2@VTES@Fc NCs, suggesting its suitable cytocompatibility (Fig. 7b). The cells treated with Fe_3O_4@SiO_2@VTES@Fc/DOX exhibited a more pronounced decrease in cell viability compared to free DOX (Fig. 7c, d). This is attributed to the effective targeting facilitated by the nanoscale size of the synthesized NPs, enabling penetration into the cancerous tissue. The results of the DAPI staining analysis indicate that Fe_3O_4@-SiO_2@VTES@Fc/DOX can induce cell apoptosis effectively and show potential as a DDS for cancer treatment.

4. Conclusion

The research developed an efficient pH-responsive core-shell magnetic nanocarrier comprising Fc and Fe_3O_4, specifically developed for potential cancer therapies. In this respect, the synthesis of Fe_3O_4 NPs was achieved using a simple co-precipitation method. Subsequently, the NPs were surface-coated with SiO_2 and VTES and then modified with Fc via a hydrosilylation process. Finally, The incorporation of ferrocene moieties on the nanoparticles significantly enhanced the drug loading capacity due to the establishment of π-π stacking interactions between DOX and the ferrocene units. The comprehensive assessment of the drug release profiles revealed that these modified nanoparticles facilitated a controlled and sustained release of DOX at acidic pH levels, simulating the tumor microenvironment, while minimizing release at physiological pH to reduce systemic toxicity. In addition, the in vitro cytotoxicity and DAPI staining demonstrated that the Fe_3O_4@SiO_2@VTES@Fc/DOX NCs exhibited greater cytotoxicity against MCF-7 cancer cells compared to free DOX. This enhanced cytotoxicity is likely due to the nanoscale size of the fabricated nanocarrier, facilitating the penetration into cancerous tissues and thereby increasing the effectiveness of the drug. Also, due to the redox activity of the ferrocene group in the synthesized Fe_3O_4@-SiO_2@VTES@Fc NCs, it shows good antioxidant properties. The results demonstrated that the proposed drug delivery system not only improves the therapeutic potential of DOX but also offers an effective strategy to target cancer therapy with greater precision.

Funding sources

This work received no external funding.

CRediT authorship contribution statement

Fahimeh Kazeminava: Formal analysis, Data curation. **Ali Mohammadzadeh:** Writing – original draft, Visualization, Software, Methodology, Investigation, Formal analysis, Data curation, Conceptualization. **Reza Mohammadi:** Supervision, Resources. **Siamak Javanbakht:** Writing – review & editing, Validation.

Declaration of Competing Interest

The authors declare that they have no known competing financial interests or personal relationships that could have appeared to influence the work reported in this paper.

Data Availability

Data will be made available on request.

Acknowledgments

This research is supported by a research grant from the University of Tabriz (number SAD/2389–14020820).

Appendix A. Supporting information

Supplementary data associated with this article can be found in the online version at doi:10.1016/j.colsurfa.2024.135201.

References

[1] A.M. Ricci, R.T. Emeny, P.J. Bagley, H.B. Blunt, M.E. Butow, A. Morgan, J. A. Alford-Teaster, L. Titus, R.R. Walston III, J.R. Rees, Causes of childhood cancer: a review of the recent literature: part I—childhood factors, Cancers (Basel) 16 (2024) 1297.
[2] K. Vyas, M. Rathod, M.M. Patel, Insight on nano drug delivery systems with targeted therapy in treatment of oral cancer, Nanomed. Nanotechnol., Biol. Med. 49 (2023) 102662.
[3] M. Pooresmaeil, S. Javanbakht, H. Namazi, A. Shaabani, Application or function of citric acid in drug delivery platforms, Med. Res. Rev. 42 (2022) 800–849.
[4] R.E. Nicoletto, C.M. Ofner, III, Cytotoxic mechanisms of doxorubicin at clinically relevant concentrations in breast cancer cells, Cancer Chemother. Pharmacol. 89 (2022) 285–311.
[5] M.I. Khan, M.I. Hossain, M.K. Hossain, M.H.K. Rubel, K.M. Hossain, A. Mahfuz, M. I. Anik, Recent progress in nanostructured smart drug delivery systems for cancer therapy: a review, ACS Appl. Bio Mater. 5 (2022) 971–1012.
[6] N.S. Elbialy, M.M. Fathy, W.M. Khalil, Doxorubicin loaded magnetic gold nanoparticles for in vivo targeted drug delivery, Int. J. Pharm. 490 (2015) 190–199.
[7] J. Goole, K. Amighi, 3D printing in pharmaceutics: a new tool for designing customized drug delivery systems, Int. J. Pharm. 499 (2016) 376–394.
[8] F.M. Kashkooli, A. Jakhmola, G.A. Ferrier, K. Sathiyamoorthy, J. Tavakkoli, M. C. Kolios, Development of an ultrasound-mediated nano-sized drug-delivery system for cancer treatment: from theory to experiment, Nanomedicine (2024) 1–23.
[9] K. Elumalai, S. Srinivasan, A. Shanmugam, Review of the efficacy of nanoparticle-based drug delivery systems for cancer treatment, Biomed. Technol. 5 (2024) 109–122.
[10] A. Mohammadzadeh, S. Javanbakht, R. Mohammadi, Magnetic alginate core-shell nanoparticles based on Schiff-base imine bonding for pH-responsive doxorubicin delivery system, Colloids Surf. A Physicochem. Eng. Asp. (2024) 134473.
[11] V. Rahimkhoei, A.H. Alzaidy, M.J. Abed, S. Rashki, M. Salavati-Niasari, Advances in inorganic nanoparticles-based drug delivery in targeted breast cancer theranostics, Adv. Colloid Interface Sci. (2024) 103204.
[12] D. Wang, Y. Li, H. Zhang, Z. Ren, K. Fan, J. Cheng, J. Zhang, F. Gao, The design of rapid self-healing alginate hydrogel with dendritic crosslinking network, Molecules 27 (2022) 7367.
[13] T. Anjum, N. Hussain, H.M.N. Iqbal, A. Jedrzak, T. Jesionowski, M. Bilal, Magnetic nanomaterials as drug delivery vehicles and therapeutic constructs to treat cancer, J. Drug Deliv. Sci. Technol. 80 (2023) 104103.
[14] R. Kumar, K. Mondal, P.K. Panda, A. Kaushik, R. Abolhassani, R. Ahuja, H.-G. Rubahn, Y.K. Mishra, Core–shell nanostructures: perspectives towards drug delivery applications, J. Mater. Chem. B 8 (2020) 8992–9027.
[15] H. Aslam, S. Shukrullah, M.Y. Naz, H. Fatima, H. Hussain, S. Ullah, M.A. Assiri, Current and future perspectives of multifunctional magnetic nanoparticles based controlled drug delivery systems, J. Drug Deliv. Sci. Technol. 67 (2022) 102946.
[16] A. Baki, F. Wiekhorst, R. Bleul, Advances in magnetic nanoparticles engineering for biomedical applications—a review, Bioengineering 8 (2021) 134.
[17] S. Shen, L. Wu, J. Liu, M. Xie, H. Shen, X. Qi, Y. Yan, Y. Ge, Y. Jin, Core–shell structured Fe3O4@ TiO2-doxorubicin nanoparticles for targeted chemo-sonodynamic therapy of cancer, Int. J. Pharm. 486 (2015) 380–388.
[18] B. Rezaei, P. Yari, S.M. Sanders, H. Wang, V.K. Chugh, S. Liang, S. Mostufa, K. Xu, J. Wang, J. Gómez-Pastora, Magnetic nanoparticles: a review on synthesis, characterization, functionalization, and biomedical applications, Small 20 (2024) 2304848.
[19] Y. Yu, Q. Xu, S. He, H. Xiong, Q. Zhang, W. Xu, V. Ricotta, L. Bai, Q. Zhang, Z. Yu, Recent advances in delivery of photosensitive metal-based drugs, Coord. Chem. Rev. 387 (2019) 154–179.
[20] Y. Xu, Y. Shan, Y. Zhang, B. Yu, Y. Shen, H. Cong, Multifunctional Fe3O4@ C-based nanoparticles coupling optical/MRI imaging and pH/photothermal controllable drug release as efficient anti-cancer drug delivery platforms, Nanotechnology 30 (2019) 425102.
[21] U. Rauf, G. Shabir, S. Bukhari, F. Albericio, A. Saeed, Contemporary developments in ferrocene chemistry: physical, chemical, biological and industrial aspects, Molecules 28 (2023) 5765.
[22] R. Zhang, X. Qin, F. Kong, P. Chen, G. Pan, Improving cellular uptake of therapeutic entities through interaction with components of cell membrane, Drug Deliv. 26 (2019) 328–342.
[23] S.-L. Li, X. Chu, H.-L. Dong, H.-Y. Hou, Y. Liu, Recent advances in augmenting Fenton chemistry of nanoplatforms for enhanced chemodynamic therapy, Coord. Chem. Rev. 479 (2023) 215004.
[24] Y. Zhou, S. Fan, L. Feng, X. Huang, X. Chen, Manipulating intratumoral fenton chemistry for enhanced chemodynamic and chemodynamic-synergized multimodal therapy, Adv. Mater. 33 (2021) 2104223.
[25] M. Patra, G. Gasser, The medicinal chemistry of ferrocene and its derivatives, Nat. Rev. Chem. 1 (2017) 66.
[26] P. Biegański, E. Kovalski, N. Israel, E. Dmitrieva, D. Trzybiński, K. Woźniak, V. Vrček, M. Godel, C. Riganti, J. Kopecka, Electronic coupling in 1, 2, 3-triazole bridged ferrocenes and its impact on reactive oxygen species generation and deleterious activity in cancer cells, Inorg. Chem. 61 (2022) 9650–9666.
[27] T. Wang, J. Hou, C. Su, L. Zhao, Y. Shi, Hyaluronic acid-coated chitosan nanoparticles induce ROS-mediated tumor cell apoptosis and enhance antitumor efficiency by targeted drug delivery via CD44, J. Nanobiotechnol. 15 (2017) 1–12.
[28] D. Venkatachalam, Y. Govindaraj, M. Prabhakar, A. Ganapathi, M. Sakairi, M. Rohwerder, L. Neelakantan, Smart release of turmeric as a potential corrosion inhibitor from a pH-responsive polymer encapsulated highly ordered mesoporous silica containers, Surf. Interfaces 45 (2024) 103883.
[29] E. Payami, A. Mohammadzadeh, K.D. Safa, R. Teimuri-Mofrad, Ferrocene surface-modified Fe3O4 nanoparticles as prominent electrode material for supercapacitor application, J. Energy Storage 88 (2024) 111624.
[30] R. Teimuri-Mofrad, F. Mirzaei, H. Abbasi, K. D. Safa, Synthesis of new binuclear ferrocenyl compounds by hydrosilylation reactions, C. R. Chim. 20 (2017) 197–205.
[31] J. Azizi, S. Javanbakht, R. Mohammadi, In-situ green synthesis of copper tannic acid framework in the presence of graphene quantum dots: improved colloidal and antibacterial properties, Int. J. Pharm. 650 (2024) 123682.
[32] W. Yin, Y. Wang, Y. Xiao, A. Mao, M. Lang, Phenylboronic acid conjugated mPEG-b-PCL micelles as DOX carriers for enhanced drug encapsulation and controlled drug release, Eur. Polym. J. 173 (2022) 111235.
[33] S. Javanbakht, M. Nabi, A. Shaabani, Graphene quantum dots-crosslinked gelatin via the efficient Ugi four-component reaction: safe photoluminescent implantable carriers for the pH-responsive delivery of doxorubicin, Materialia 20 (2021) 101233.
[34] H. Hamedi, S. Javanbakht, R. Mohammadi, In-situ synthesis of copper-gallic acid metal–organic framework into the gentamicin-loaded chitosan hydrogel bead: a synergistic enhancement of antibacterial properties, J. Ind. Eng. Chem. 133 (2024) 454–463.
[35] S. Karimi, H. Namazi, Synthesis of folic acid-conjugated glycodendrimer with magnetic β-cyclodextrin core as a pH-responsive system for tumor-targeted co-delivery of doxorubicin and curcumin, Colloids Surf. A Physicochem. Eng. Asp. 627 (2021) 127205.
[36] A. Saboury, R. Mohammadi, S. Javanbakht, M. Ghorbani, Doxorubicin imprinted magnetic polymethacrylamide as a pH-sensitive anticancer nanocarrier, J. Drug Deliv. Sci. Technol. 79 (2023) 103998.
[37] L. Zhang, Y. Zhang, Y. Wu, Y. Cao, X. Wu, Y. Xu, H. Yu, Y. Jiao, J. Yu, L. Wang, Advancing water treatment: harnessing cyclodextrin metal-organic frameworks with dual protonation sites for enhanced sulfate adsorption efficiency, Colloids Surf. A Physicochem. Eng. Asp. 691 (2024) 133835.
[38] S. Azadi, E. Azizipour, A.M. Amani, A. Vaez, Z. Zareshahrabadi, A. Abbaspour, T. Firuzyar, H. Dortaj, H. Kamyab, S. Chelliapan, Antifungal activity of Fe3O4@ SiO2/Schiff-base/Cu (II) magnetic nanoparticles against pathogenic Candida species, Sci. Rep. 14 (2024) 5855.
[39] E. Mandev, S. Rahimpour, A. Mohammadzadeh, B. Sahin, F. Afshari, R. Teimuri-Mofrad, Surface modification of Fe 3 O 4 nanoparticles for preparing stable water-based nanofluids, Heat. Transf. Res. 53 (2022).
[40] E. Payami, M.A. Keynezhad, K.D. Safa, R. Teimuri-Mofrad, Development of high-performance supercapacitor based on Fe3O4@ SiO2@ PolyFc nanoparticles via surface-initiated radical polymerization, Electrochim. Acta 439 (2023) 141663.
[41] Y. Liu, K. Li, Y. Wu, J. Ma, P. Tang, Y. Liu, D. Wu, PVA reinforced gossypolone and doxorubicin π–π stacking nanoparticles towards tumor targeting and ultralow dose synergistic chemotherapy, Biomater. Sci. 7 (2019) 3662–3674.
[42] L. Danyang, D. Yimin, Z. Jiaqi, W. Shengyun, L. Qi, C. Ling, Sandwich-type ferrocene-functionalized magnetic nanoparticles: synthesis, characterization, and the adsorption of Cr (VI), J. Mater. Sci. Mater. Electron. 30 (2019) 13924–13932.
[43] E. Kianfar, Magnetic nanoparticles in targeted drug delivery: a review, J. Supercond. Nov. Magn. 34 (2021) 1709–1735.
[44] A. Spoială, C.-I. Ilie, L. Motelica, D. Ficai, A. Semenescu, O.-C. Oprea, A. Ficai, Smart magnetic drug delivery systems for the treatment of cancer, Nanomaterials 13 (2023) 876.
[45] A. Pusta, M. Tertis, I. Crăciunescu, R. Turcu, S. Mirel, C. Cristea, Recent advances in the development of drug delivery applications of magnetic nanomaterials, Pharmaceutics 15 (2023) 1872.

[46] Y. Luo, X. Yao, J. Yuan, T. Ding, Q. Gao, Preparation and drug controlled-release of polyion complex micelles as drug delivery systems, Colloids Surf. B Biointerfaces 68 (2009) 218–224.
[47] N. Farmanbar, S. Mohseni, M. Darroudi, Green synthesis of chitosan-coated magnetic nanoparticles for drug delivery of oxaliplatin and irinotecan against colorectal cancer cells, Polym. Bull. 79 (2022) 10595–10613.
[48] J. Cheng, Y. Zhang, Y. Liu, Supramolecular assembly of thiolated cyclodextrin and ferrocene derivative for controlled drug delivery, ChemNanoMat 4 (2018) 758–763.
[49] H. Jafari, H. Namazi, pH-sensitive biosystem based on laponite RD/chitosan/polyvinyl alcohol hydrogels for controlled delivery of curcumin to breast cancer cells, Colloids Surf. B Biointerfaces 231 (2023) 113585.
[50] S. Javanbakht, A. Saboury, A. Shaabani, R. Mohammadi, M. Ghorbani, Doxorubicin imprinted photoluminescent polymer as a pH-responsive nanocarrier, ACS Appl. Bio Mater. 3 (2020) 4168–4178.